



Northern Illinois  
University

# Search for Charged Higgs Bosons in the $\tau^\pm \nu_\tau$ Final State with $139\text{ fb}^{-1}$ of pp Collision Data at $\sqrt{s} = 13\text{ TeV}$ with the ATLAS Experiment

Dissertation Defense

Elliot Parrish<sup>†</sup>

<sup>†</sup>Northern Illinois University, USA

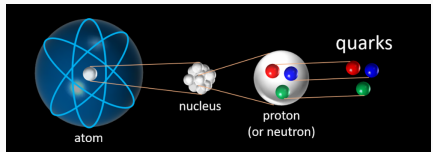
October 13, 2022

Introduction	Experimental Apparatus	$H^\pm \rightarrow \tau^\pm \nu_\tau$	$H^\pm \rightarrow \tau^\pm \nu_\tau$
Theory		Background	PNN
The Standard Model	LHC	Modeling	PNN HPO
New Physics	ATLAS	MVA	Systematic
Charged Higgs Bosons	Object Reconstruction	JHEP 09(2018)139	Uncertainties Results
	Simulation	Results	Conclusion

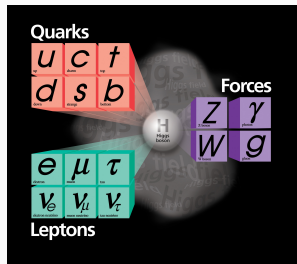
- This defense will take  $\approx 1$  hour
  - I will walk you through the work that is contained in my PhD dissertation
  - After the presentation is complete, there will be time for public questions, then the committee and I will address comments privately
  - When we are done, I will return, the committee will discuss among themselves then return
- General Guidelines
  - Please remain muted unless you are speaking
  - There will be time at the end for questions, but feel free to interrupt if there is something urgent
- Thank you for attending!

# What are we made of?

- The scientific field of particle physics seeks to explain the building blocks of the universe
  - How many fundamental particles are there?
  - How do they interact with each other?
- The Standard Model of Particle Physics (SM)
  - Matter is comprised of fermions
    - Quarks combine to create hadrons (protons, neutrons,  $\pi^{\pm,0}$ , etc)
  - Forces are carried by an exchange of bosons
    - Gluon ( $g$ ) → Strong force
    - Photon ( $\gamma$ ) → Electromagnetism
    - $W^\pm, Z^0$  → Weak force
    - No explicit mass terms



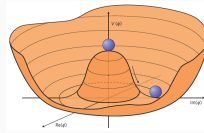
[1] [2]



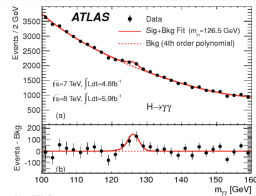
# The Higgs Boson



- At high energies, electromagnetism and the weak forces are one “electroweak” force
- Higgs field exists everywhere in space
  - Non-zero vacuum expectation value
    - Electroweak symmetry breaking
- Interaction with Higgs field gives mass
- Discovered jointly by the ATLAS and CMS collaborations in 2012



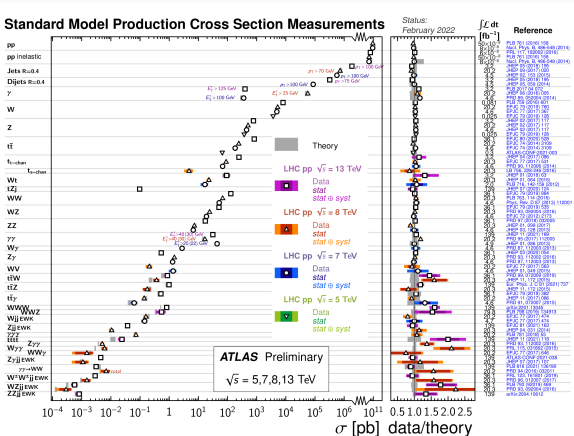
[3]



[4]

# The Standard Model

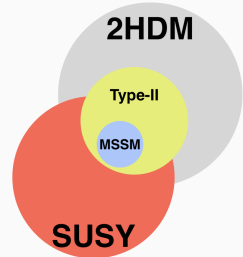
- Predicts the probabilities of creation and decay of particles (among many other things)
  - Has been thoroughly tested
  - Measurements agree to a high degree of accuracy
- Not a complete theory (Not a full list)
  - Gravity
  - Matter-antimatter asymmetry in the universe
  - Hierarchy problem
    - EW scale is  $\sim 100$  GeV
    - Planck scale is  $\sim 10^{18}$  GeV



# Beyond the Standard Model



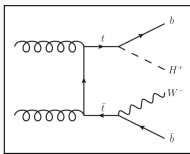
- 2 Higgs Doublet Models and Supersymmetry (SUSY) are large groups of theories attempting to address these issues
  - 2HDM have two complex doublet scalar fields [5]
    - Two relevant free parameters,  $\tan \beta$  and  $m_{H^\pm}$
    - $\tan \beta$  is the ratio of the vacuum expectation values of the two doublets
  - SUSY proposes a symmetry between fermions and bosons
    - Many new possible particles
    - Minimal Supersymmetric Standard Model (MSSM) is the smallest SUSY extension to the SM



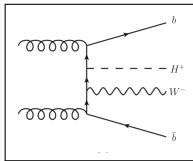
light neutral scalar	$h^0$
heavy neutral scalar	$H^0$
neutral pseudoscalar	$A^0$
two charged scalars	$H^\pm$

# Charged Higgs Bosons

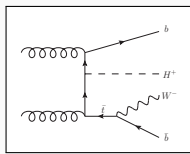
- At the LHC, theoretical production mode of  $m_{H^\pm}$  is mainly in top-quark decays or in association with a top-quark ( $t$ )
  - $H^\pm$  production mode is dependent on  $m_{H^\pm}$



$$m_{H^\pm} < m_t$$

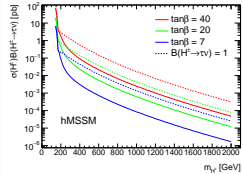


$$m_{H^\pm} \simeq m_t$$

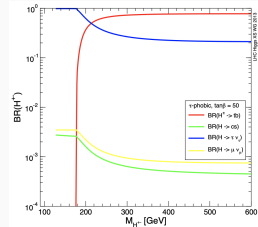


$$m_{H^\pm} > m_t$$

- $H^\pm \rightarrow \tau^\pm \nu_\tau$  decay channel remains significant for high  $\tan \beta$

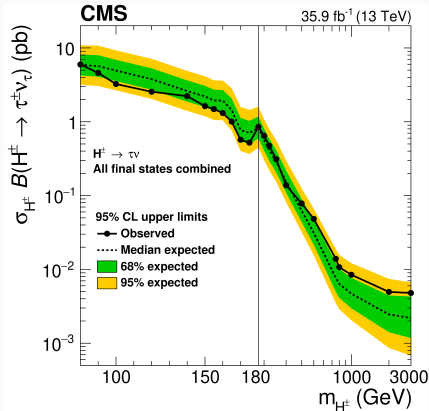


[6]

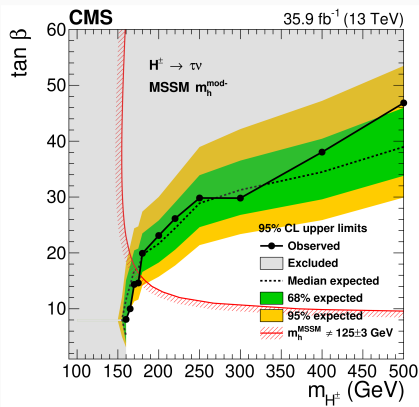


[7]

# Other $H^\pm \rightarrow \tau^\pm \nu_\tau$ Searches



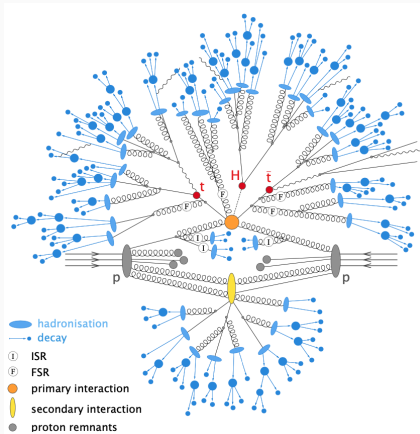
[8]



[8]

# Particle Collisions

- Most particles we are interested in are not stable and cannot be observed in our environment
- Collide known particles to study them and potentially new particles
  - $E^2 = m^2 c^4 + p^2 c^2$
- Hadronization
  - Quarks cannot exist on their own
  - Must combine to form bound states
  - Combine shower into a jet



[9]

# Large Hadron Collider

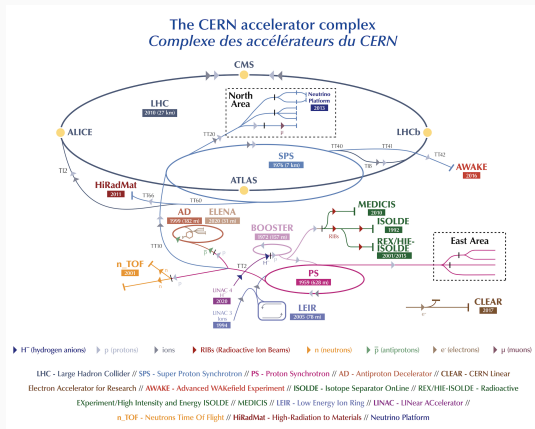


- Largest particle collider ever built
- Highest energy particle collider
- Located at CERN outside of Geneva, Switzerland
- Four main collision points
  - **ATLAS**, ALICE, CMS, LHCb

Selected Run-2 LHC Parameters

Circumference	26,659 m
Magnet operating temperature	1.9 K
Beam energy	6.5 TeV (13 CM TeV)
Protons per bunch	$1.2 \times 10^{11}$
Bunches per beam	2808
Speed of bunches	> 1,000,000,000 km/hr ( $\simeq 99.999\% c$ )

[10]

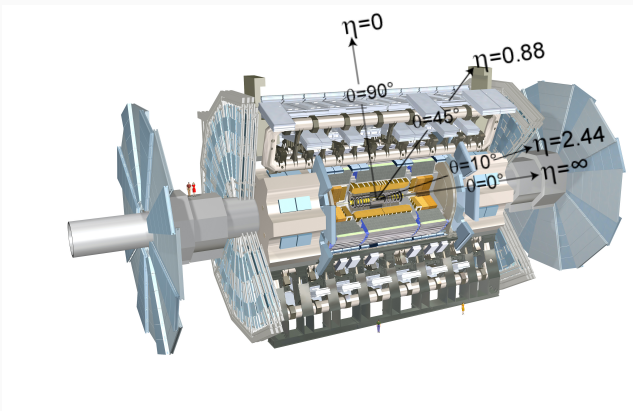


[11]

# The ATLAS Detector



- General purpose particle detector
  - Magnet System
  - Tracker
  - Calorimeters
  - Muon Spectrometer
- Coordinate system origin at interaction point
  - $r$  is radial distance
  - $\eta \equiv -\ln(\tan(\frac{\theta}{2}))$
  - $\phi$  is azimuthal angle

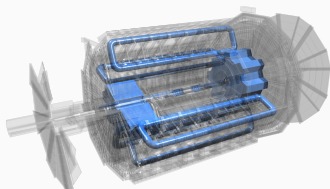


[12] [13]

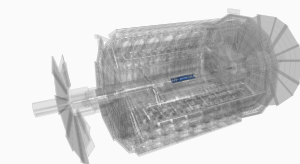
# Magnet System and Inner Detector



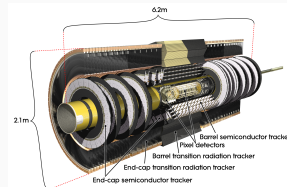
- Central solenoid
  - 2 T magnetic field
  - Bends charged particles in transverse plane
- Toroid system
  - 3.9 T magnetic field
  - Bends charged particles ( $\mu$ ) along beam axis



- Inner detector (ID)
  - Tracks trajectories of charged particles
  - Used to measure momentum in the transverse plane ( $p_T$ )

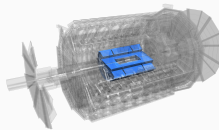
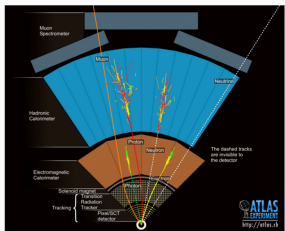


[12]

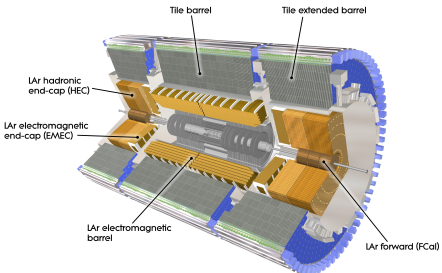


# Calorimeters

- Important in jet,  $\tau$ ,  $E_T^{\text{miss}}$  and  $\mu$  identification and triggering
- Measure energy of charged particles
  - Designed to fully absorb particles



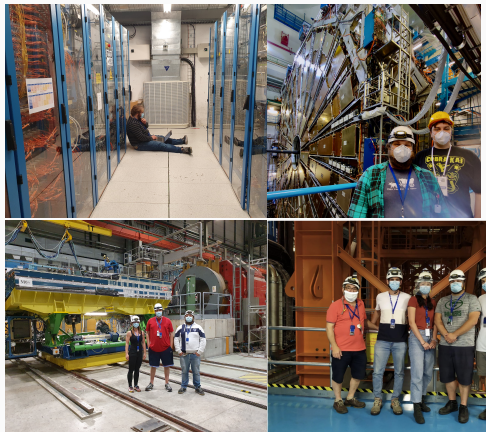
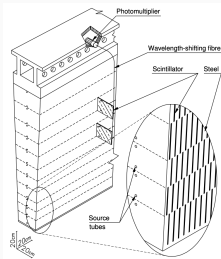
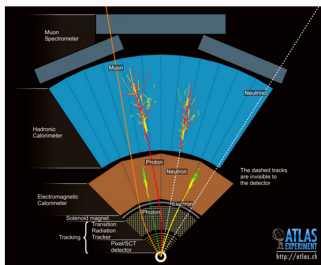
[12]



# Tile Calorimeter



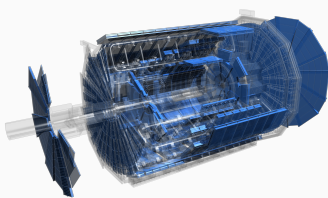
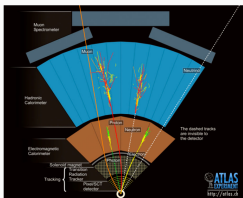
- Scintillating tile with steel absorber
- I served as Data Quality Co-Coordinator for several years
  - In Run-2 99.65% DQ efficiency [14]



# Muon System and Trigger



- Muon Spectrometers (MS) detect and measure  $\mu$ 
  - Muons are minimally ionizing
  - $\mu$  reach the outermost region of the detector
  - Information combined with inner detector to reconstruct  $\mu$

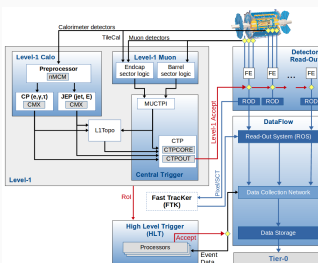


Search for  $H^\pm \rightarrow \tau^\pm \nu_\tau$  with ATLAS

Experimental Apparatus ATLAS

## Trigger System

- Need to quickly sort through data and decide if a collision is interesting or not
- Mix of hardware and software



[16]

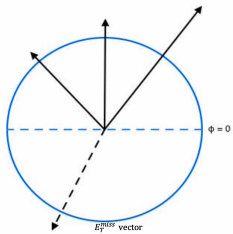
Elliot Parrish (NIU)

16 / 43

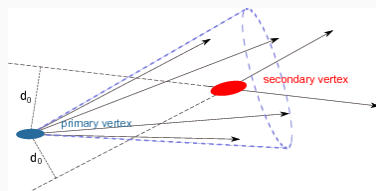
# Reconstruction: $E_T^{\text{miss}}$ and $b$ -jets



- Particles like  $\nu$  do not leave a signature within ATLAS
- Instead, infer their presence through momentum conservation
  - Negative vector sum of all objects in a collision event



- $b$  quark initiated hadronic showers are identified by a displaced vertex, etc.
- Reconstructed as a jet, tagged as a  $b$ -jet
  - Algorithms designed to identify  $b$ -jets called taggers [17]

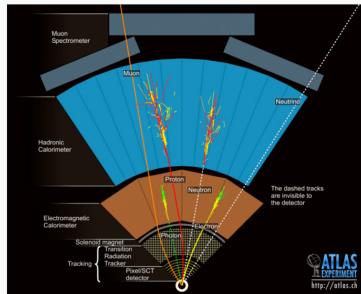


[18]

# Reconstruction: $e$ and $\mu$

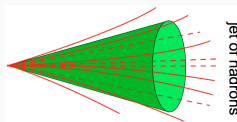
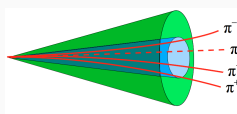


- Electron identification
  - Information from the ID and showers in the EM calorimeter are combined
  - This analysis uses tight ID and tight isolation requirements
- $\mu$  identification
  - Information from the ID is combined with the MS
  - This analysis uses tight ID and tight isolation requirements



# Reconstruction: $\tau$ leptons

- $\tau$  leptons typically decay before they interact with the detector
- $\tau$  leptons decay hadronically  $\approx 65\%$  of the time
  - leptonic decays are not considered
- Number of charged hadrons ( $\pi^\pm$ ) in decays defines number of prongs
  - 1  $\pi^\pm$  occurs 72% of the time
  - 3  $\pi^\pm$  occurs 22% of the time
  - Of these decays, 68% contain  $> 1 \pi^0$
- $\nu_\tau$  are also produced in these decays
  - Only visible part of  $\tau$  can be reconstructed

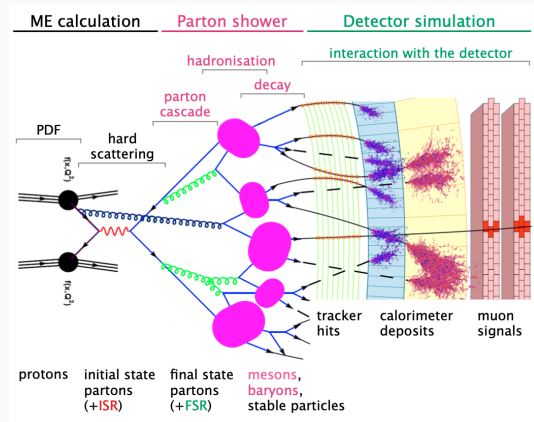


[19]

- Reconstruction is imperfect
  - Misidentification of particles is a large source of background

# Simulation

- Incredibly detailed simulations are used to create analysis strategy
  - Entire data flow from collision to detector readout is simulated
  - Many different options to generate simulations
    - Some excel at specific tasks and not great at others
- Control regions are used to verify simulation agreement with data



[9]

# Analysis Overview

- Search for singly charged  $H^\pm$  decaying to  $\tau^\pm \nu_\tau$  over a wide mass range
  - Low mass ( $m_{H^\pm} < m_t$ ):
  - Intermediate mass\* ( $m_{H^\pm} \simeq m_t$ )
  - High mass ( $m_{H^\pm} > m_t$ )

- Dominant backgrounds

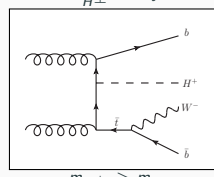
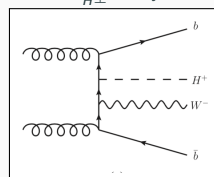
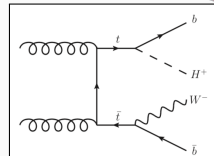
Backgrounds w/ prompt hadronic $\tau$	Backgrounds w/ fake $\tau$
$t\bar{t}$ estimated with simulation	Fake $j \rightarrow \tau$ estimated with data driven fake factor method
$V + jets$ estimated with simulation	Fake $\ell \rightarrow \tau$ estimated with simulation, validated on $Z \rightarrow ee$
$VV$ estimated with simulation	

- Classifier score is used as the final discriminant

- Two sub-channels based on the decay mode of associated  $t$

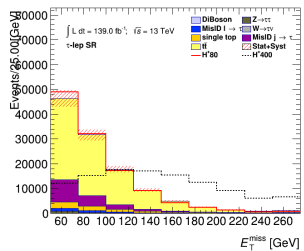
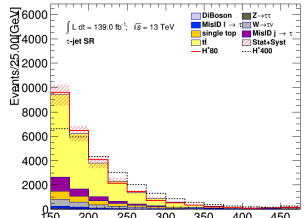
Sensitive at high mass due to higher  $W \rightarrow q\bar{q}$  BR      Sensitive at low mass due to easier triggering

\*: First time probed experimentally [JHEP 09\(2018\)139](#)



# Background Estimation

- Signal region  $E_T^{\text{miss}}$  distributions on right show background composition
- Define control regions to verify main sources of background

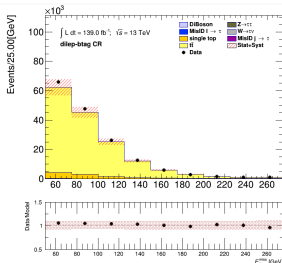
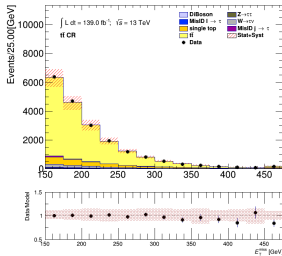


# Background Estimation

- Signal region  $E_T^{\text{miss}}$  distributions on right show background composition
- Define control regions to verify main sources of background

Background Modeling	$\tau + \text{jets}$	Control Regions	$\tau + \ell$ Control Regions	Data/Model Agreement
$t\bar{t} + \text{single top}$	$t\bar{t}$	Dilepton-btag		✓

- Estimated with simulation

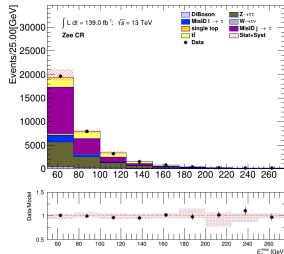
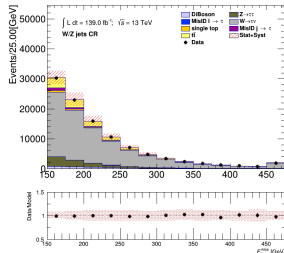


# Background Estimation

- Signal region  $E_T^{\text{miss}}$  distributions on right show background composition
- Define control regions to verify main sources of background

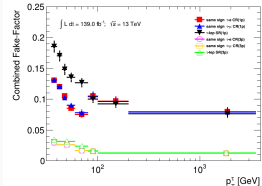
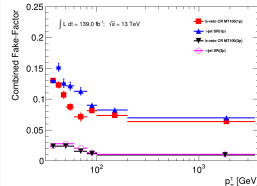
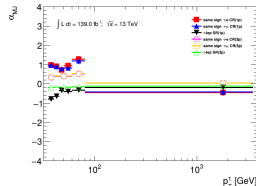
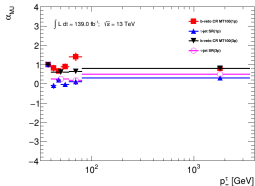
Background Modeling	$\tau + \text{jets}$	Control Regions	$\tau + \ell$ Control Regions	Data/Model Agreement
$t\bar{t} + \text{single top}$	$t\bar{t}$	Dilepton-btag	✓	
V+Jets	W+Jets	Zee (Fake $\ell \rightarrow \tau$ enriched)	✓	

- Estimated with simulation



# Background Estimation: $j \rightarrow \tau$ Fakes

- $j \rightarrow \tau$  fakes estimated with a data-driven fake factor (FF) method (from Multijet and W+jets)
  - Anti-selection of  $\tau$  that fail  $\tau$  ID but pass looser selection
  - Define CRs to extract fake factors
  - Subtract SM contribution from simulation
  - $FF = \frac{N_{fake\tau}}{N_{anti-\tau}}$
- In SR, measure fraction of fakes ( $\alpha$ ) using template fit of  $\tau$  ID score distributions using template shapes from  $anti - \tau$  distributions in CRs
- $FF_{sig} = \alpha_{MJ} \times FF_{MJ} + (1 - \alpha_{MJ}) \times FF_{W+jets}$
- In SR,  $N_{fake\tau} = FF_{sig} \times N_{anti-\tau}$

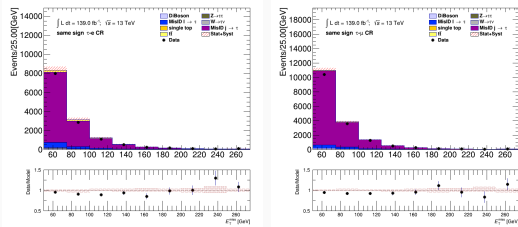
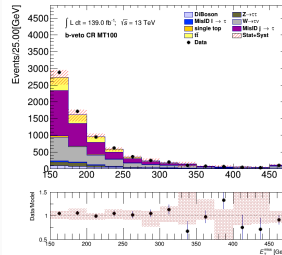


# Background Estimation: $j \rightarrow \tau$ Fakes

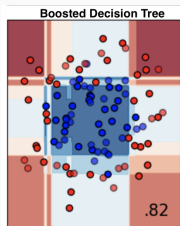
- Signal region  $E_T^{\text{miss}}$  distributions on right show background composition
- Define control regions to verify main sources of background

Background Modeling	$\tau + \text{jets}$ Control Regions	$\tau + \ell$ Control Regions	Data/Model Agreement
$t\bar{t} + \text{single top}$	$t\bar{t}$	Dilepton-btag	✓
Fake $j \rightarrow \tau$ enriched	$b$ veto $m_T(\tau, E_T^{\text{miss}}) > 100$	Same Sign	✓

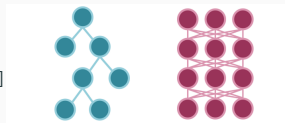
- Estimated with a data-driven fake factor method



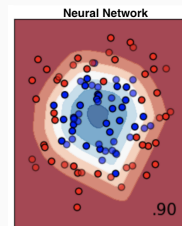
- Boosted Decision Tree (BDT)
  - Cascading decisions bin parameter space to optimize accuracy
  - Deterministic approach



[20]



- Neural Networks
  - Network of connected nodes of activation functions connected by weights
  - Probabilistic approach



[21]

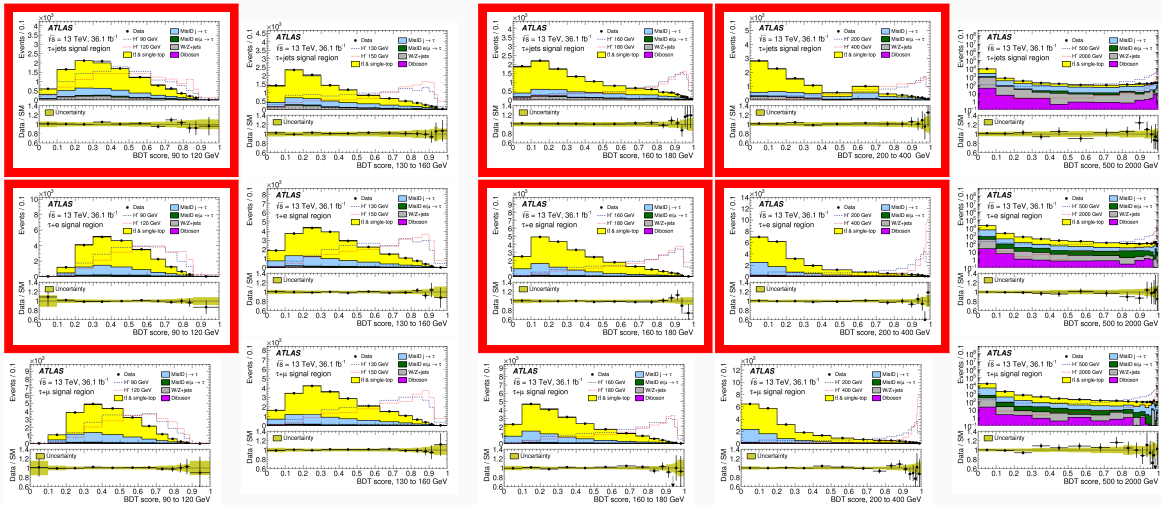
[20]

- Background modeling and classifier training kept statistically independent via the k-fold method
- BDTs binned in  $m_{H^\pm}$ 
  - 90-120, 130-160, 160-180, 200-400, 500-2000 GeV
  - Trained separately on  $\tau + \text{jets}$  and  $\tau + \ell$
  - Independent trainings for 1 or 3  $\tau$  tracks
  - $\tau + \ell$  trained inclusively, evaluated separately on  $\tau + e$  and  $\tau + \mu$
- At low  $m_{H^\pm}$ ,  $\tau$  polarization is important
  - $\Upsilon = \frac{E_T^{\pi^\pm} - E_T^{\pi^0}}{E_T^\tau} \approx 2 \frac{p_T^{\tau-\text{track}}}{p_T^\tau} - 1$
  - Only defined for 1 track  $\tau$  candidates
- At high,  $m_{H^\pm}$   $\Upsilon$  becomes less important
  - $E_T^{\text{miss}}$ ,  $p_T^\tau$ , and  $\Delta\phi_{\tau, E_T^{\text{miss}}}$  have higher discriminating power

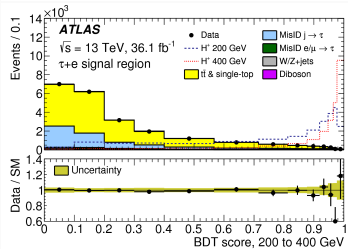
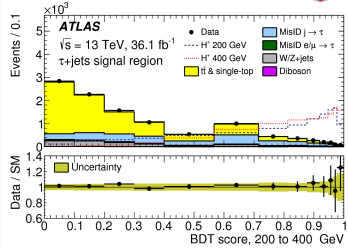
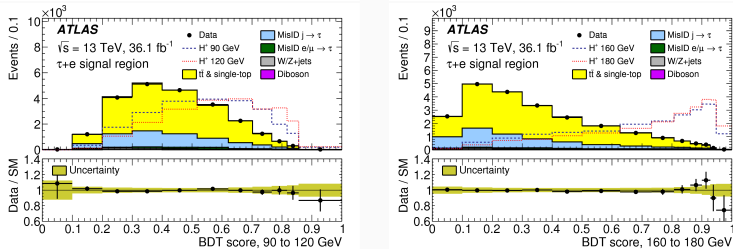
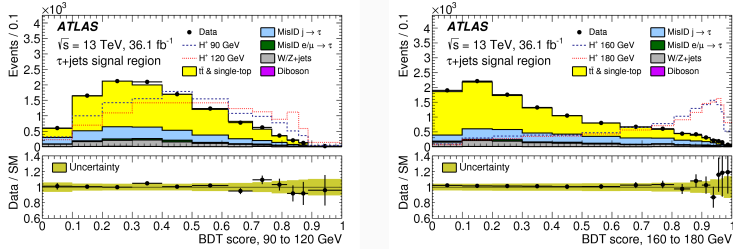
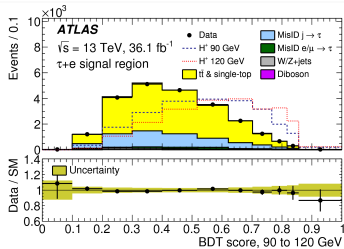
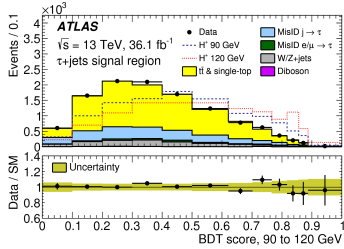
	Fold 1	Fold 2	Fold 3	Fold 4	Fold 5	Background
Partition 1	Evaluation	Train	Train	Train	Train	Fold 1
Partition 2	Train	Evaluation	Train	Train	Train	Fold 2
Partition 3	Train	Train	Evaluation	Train	Train	Fold 3
Partition 4	Train	Train	Train	Evaluation	Train	Fold 4
Partition 5	Train	Train	Train	Train	Evaluation	Fold 5

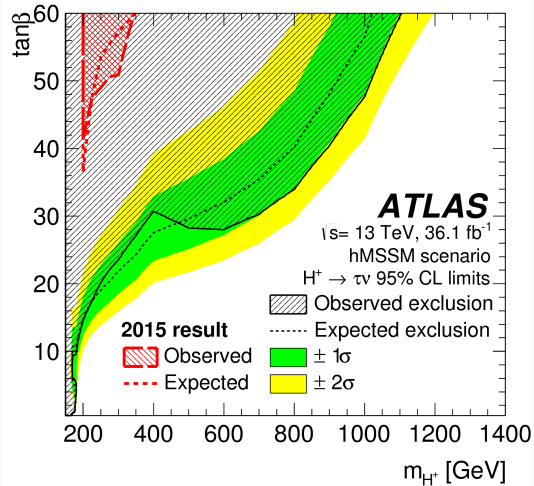
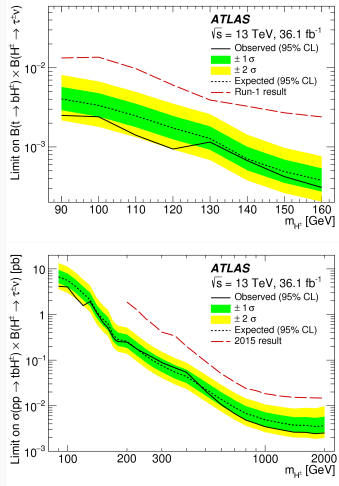
MVA input variable	$\tau + \text{jets}$	$\tau + \ell$
$E_T^{\text{miss}}$	✓	✓
$p_T^\tau$	✓	✓
$p_T^{b-jet}$	✓	✓
$\Delta\phi(\tau, E_T^{\text{miss}})$	✓	✓
$\Delta\phi(b-jet, E_T^{\text{miss}})$	✓	✓
$\Delta R(b-jet, \tau)$	✓	
$p_T^l$		✓
$\Delta\phi(l, E_T^{\text{miss}})$		✓
$\Delta R(\tau, l)$		✓
$\Delta R(b-jet, l)$		✓
$\frac{\Delta\phi(\tau, E_T^{\text{miss}})}{\Delta\phi(jet, E_T^{\text{miss}})}$	✓	✓
$\Upsilon = 2 \frac{p_T^{\tau-\text{track}}}{p_T^\tau} - 1$	< 500 GeV	< 500 GeV

# JHEP 09(2018)139 BDT Scores in Signal Regions



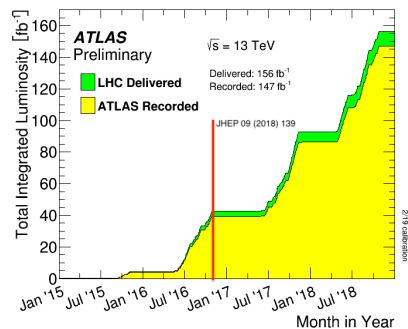
# JHEP 09(2018)139 BDT Scores in Signal Regions





# Updates to analysis since last publication

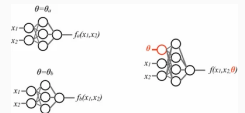
- Signal mass range extended
  - Previous:  $90 \leq m_{H^\pm} \leq 2000$  GeV
  - Current:  $80 \leq m_{H^\pm} \leq 3000$  GeV
- Increased statistics of signal due to optimized simulation generation
- New analysis framework centered around using modern Machine Learning tools
- Investigated new multivariate analysis techniques
- Improved particle identification algorithms
- Almost 4× more data



[22]

# Parameterized Neural Networks

- Parameterized Neural Networks (PNNs) can be trained and evaluated on entire  $m_{H^\pm}$  range
  - PNN learns more information with the same amount of data
    - PNN can be evaluated on mass points that are not simulated
    - Detailed information here: [arXiv:1601.07913](https://arxiv.org/abs/1601.07913)
- Background modeling and classifier training kept statistically independent via the k-fold method ( $k = 5$ )
- Trained using simulation for backgrounds with true  $\tau$ 
  - Separate models trained on 1 prong and 3 prong  $\tau$ 
    - $\tau$  polarization used to enhance low  $m_{H^\pm}$  performance
    - $\Upsilon = \frac{E_T^\pi \pm - E_T^\pi{}^0}{E_T^\pi} \approx 2 \frac{p_T^\tau - \text{track}}{p_T^\tau} - 1$
    - $\tau + \ell$  channel is trained inclusive for  $\tau + e$  and  $\tau + \mu$

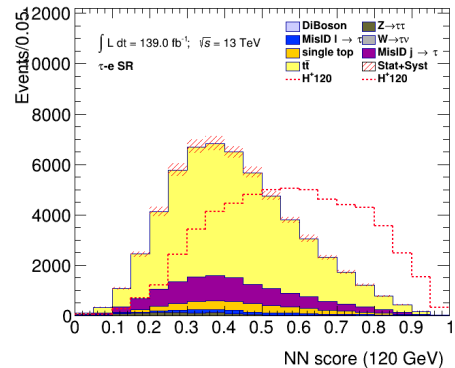
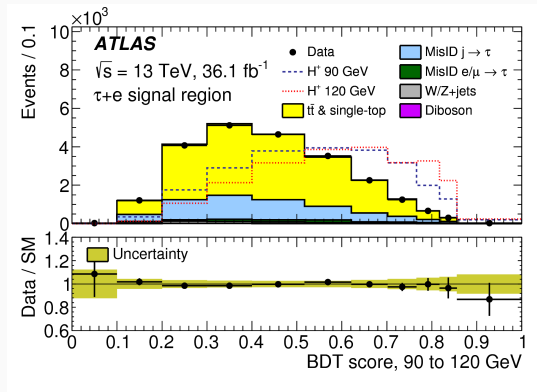


[23]

$\tau + \ell$ Input Variables		
$p_T^\tau$	$\eta^\tau$	$\phi^\tau$
$p_T^\ell$	$\eta^\ell$	$\phi^\ell$
$p_T^{j_0}$	$\eta^{j_0}$	$\phi^{j_0}$
$E_T^{\text{miss}}$	$\phi^{E_T^{\text{miss}}}$	$p_T^h$
$m_{\text{Truth}}^{H^\pm}$	$\Upsilon^\tau$	

$\tau + \text{jets}$ Input Variables		
$p_T^\tau$	$\eta^\tau$	$\phi^\tau$
$p_T^{j_0}$	$\eta^{j_0}$	$\phi^{j_0}$
$p_T^{j_1}$	$\eta^{j_1}$	$\phi^{j_1}$
$p_T^{j_2}$	$\eta^{j_2}$	$\phi^{j_2}$
$E_T^{\text{miss}}$	$\phi^{E_T^{\text{miss}}}$	$m_{\text{Truth}}^{H^\pm}$
$\Upsilon^\tau$		

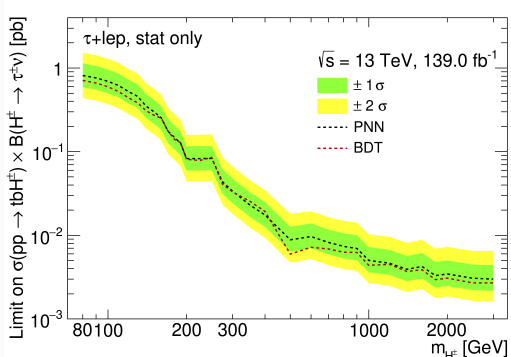
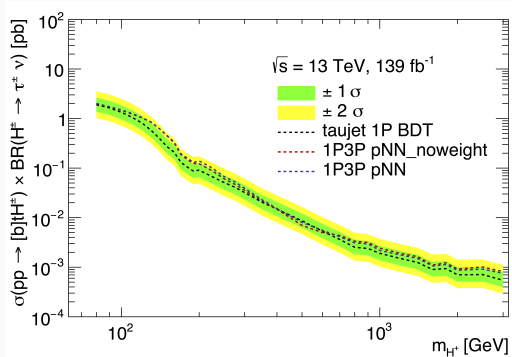
# Boosted Decision Tree vs Parameterized Neural Network



# Boosted Decision Tree vs Parameterized Neural Network



- These comparisons were done with an optimized BDT and an unoptimized PNN
- PNN chosen as classifier



# PNN Input Variable Selection



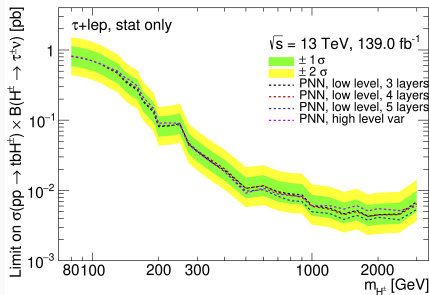
**Low Level Input Variables**

$p_T^\tau$	$\eta^\tau$	$\phi^\tau$
$p_T^\ell$	$\eta^\ell$	$\phi^\ell$
$p_T^{b-jet}$	$\eta^{b-jet}$	$\phi^{b-jet}$
$p_T^{jet}$	$\eta^{jet}$	$\phi^{jet}$
$E_T^{\text{miss}}$	$\phi_E^{\text{miss}}$	$p_T^h$
$\Upsilon$	$m_{H^\pm}^{\text{Truth}}$	

**High Level Input Variables**

$p_T^\tau$	$p_T^{b-jet}$	$p_T^\ell$
$E_T^{\text{miss}}$	$\Delta\phi_{\tau, \text{miss}}$	$\Delta\phi_{b-jet, \text{miss}}$
$\Delta\phi_{\ell, \text{miss}}$	$\Delta R_{\tau, \ell}$	$\Delta R_{b-jet, \ell}$
$\Delta R_{b-jet, \tau}$	$\Delta\phi_{\tau, \text{miss}}/\Delta\phi_{jet, \text{miss}}$	$\Upsilon$
$m_{H^\pm}^{\text{Truth}}$		

- Comparison between raw input variables and engineered variables
- Expected limits in the  $\tau + \ell$  subchannel was used as figure of merit
- Low level variables best at high  $m_{H^\pm}$



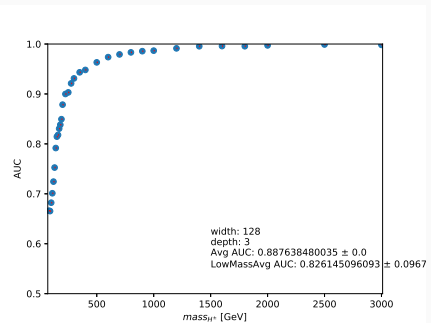
- Performed in the  $\tau + \ell$  sub-channel
- Used area under curve (AUC) of scores as figure of merit
  - Averaged over 5 kfolds, standard deviation is taken from kfolds
  - Average Area Under the Curve (AUC) from 80 GeV to 500 GeV to optimize for low mass
- Used early stopping for training
  - $\Delta_{min} = 0.00001$  and a patience of 10
  - Best weights were kept
- To speed up hyperparameter optimization (HPO), ran multiple small grids of hyperparameters
  - Scan over activation functions and loss functions
  - Scan over dropout value
  - Scan over activation function
  - Scan over LeakyReLU  $\alpha$
  - Fixed alpha over more widths and depths

# Final PNN Model Performance



Layers	Number of Neurons	Loss Function	Activation Function	LeakyReLu $\alpha$	Dropout
3	128	Binary Crossentropy	LeakyReLu	0.1	0.1

width	depth	LowMassAvg
128	3	$0.8261 \pm 0.0968$
128	5	$0.8235 \pm 0.1000$
128	4	$0.8232 \pm 0.0994$
128	2	$0.8231 \pm 0.1006$
64	4	$0.8230 \pm 0.0994$
64	2	$0.8228 \pm 0.0996$
64	5	$0.8224 \pm 0.0997$
64	3	$0.8223 \pm 0.0994$
256	5	$0.8213 \pm 0.1003$
256	4	$0.8181 \pm 0.1013$
32	3	$0.8139 \pm 0.1031$
32	4	$0.8139 \pm 0.1031$
32	2	$0.8135 \pm 0.1023$
32	5	$0.8128 \pm 0.1035$
256	2	$0.8120 \pm 0.1023$



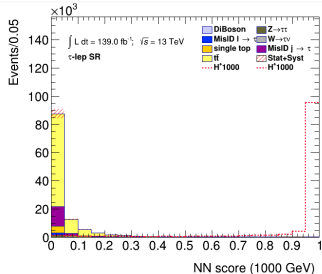
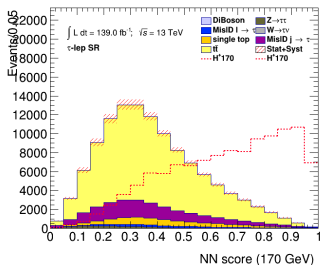
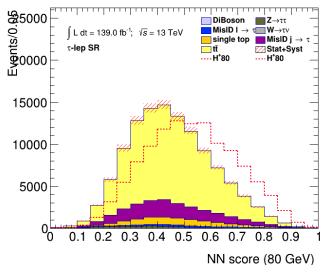
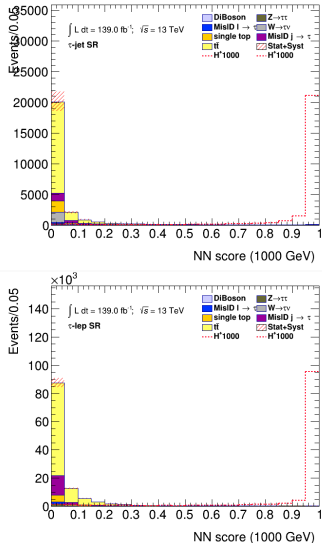
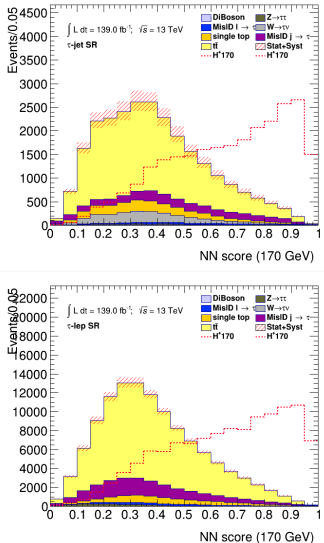
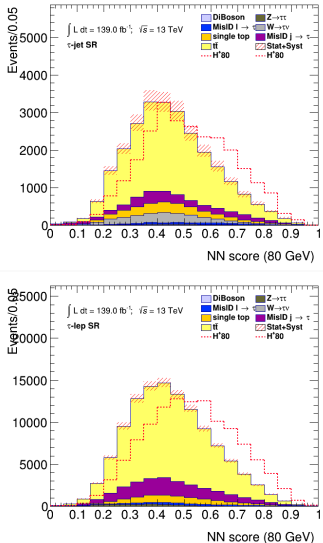
# Sources of Systematic Uncertainty



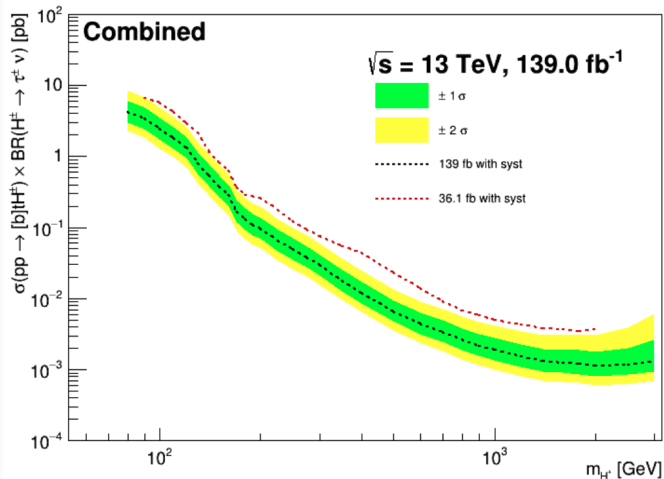
- Errors shown in plots include systematic uncertainties
  - Signal and  $t\bar{t}$  theory uncertainties are not included
  - Studies are being finalized

Source	Impact on the expected event yield (%)					
	$\tau + \text{jets}$		$\tau + e$		$\tau + \mu$	
	$t\bar{t}$	$H^\pm$ 200 GeV	$t\bar{t}$	$H^\pm$ 200 GeV	$t\bar{t}$	$H^\pm$ 200 GeV
Fake factor uncertainties	+8.23 -8.15	+8.23 -8.15	+7.58 -7.74	+7.58 -7.74	+7.58 -7.74	+7.58 -7.74
jet uncertainties	+7.38 -8.39	+6.51 -9.06	+3.41 -3.31	+4.49 -2.78	+3.18 -3.24	+3.67 -2.96
$\tau$ uncertainties	$\pm 4.36$	+2.91 -2.80	+2.84 -2.74	+2.65 -2.70	+2.77 -2.78	+2.58 -2.97
$E_T^{\text{miss}}$ uncertainties	+1.31 -1.12	+1.15 -1.49	+0.29 -0.24	+0.88 -0.34	+0.30 -0.23	+0.21 -0.11
trigger uncertainties	+1.23 -1.61	$\pm 0.03$	0	0	+0.55 -0.56	$\pm 0.56$
$e$ uncertainties	0	0	$\pm 0.71$	$\pm 0.73$	0	0
$\mu$ uncertainties	0	0	-0.01	-0.11	+0.97 -1.41	+1.08 -2.96

# PNN Results



# $H^\pm \rightarrow \tau\nu$ Expected Limits

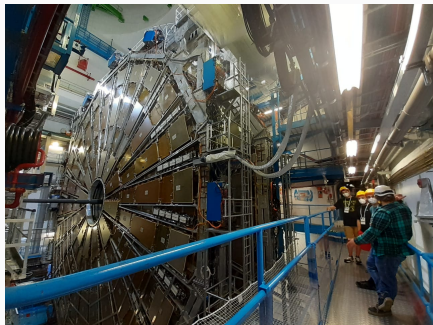


Combined  $\tau + \text{jets}$  and  $\tau + \ell$  signal regions

# Conclusions



- A search for  $H^\pm \rightarrow \tau^\pm \nu_\tau$  was improved upon
- Investigated, optimized, and implemented modern machine learning techniques
- New analysis strategy outperforms previous analysis by  $\gtrsim 3\times$
- Analysis is still blinded and work is ongoing towards a publication



# Thank You



## References i

- [1] D. Hemphill, *The behavior of the primordial universe*, Apr. 2020. [Online]. Available:  
[https://www.physics.purdue.edu/about/prizes\\_awards/charlotte\\_ida\\_litman\\_tubis\\_award/2017\\_behavior\\_primordial\\_universe.html](https://www.physics.purdue.edu/about/prizes_awards/charlotte_ida_litman_tubis_award/2017_behavior_primordial_universe.html).
- [2] D. Leah, *The standard model: The most successful theory ever*, [Online]. Available: <https://news.fnal.gov/2011/11/the-standard-model-the-most-successful-theory-ever/>.
- [3] J. Ellis, “Higgs Physics,” 117–168. 52 p, Dec. 2013, 52 pages, 45 figures, Lectures presented at the ESHEP 2013 School of High-Energy Physics, to appear as part of the proceedings in a CERN Yellow Report. DOI: 10.5170/CERN-2015-004.117. arXiv: 1312.5672. [Online]. Available: <https://cds.cern.ch/record/1638469>.

## References ii

- [4] ATLAS Collaboration, "Observation of a new particle in the search for the standard model higgs boson with the atlas detector at the lhc," *Physics Letters B*, vol. 716, no. 1, pp. 1–29, 2012.
- [5] G. Branco, P. Ferreira, L. Lavoura, M. Rebelo, M. Sher, and J. P. Silva, "Theory and phenomenology of two-higgs-doublet models," *Physics Reports*, vol. 516, no. 1–2, pp. 1–102, Jul. 2012, ISSN: 0370-1573. DOI: 10.1016/j.physrep.2012.02.002. [Online]. Available: <http://dx.doi.org/10.1016/j.physrep.2012.02.002>.
- [6] The ATLAS Collaboration, "Search for charged Higgs bosons decaying via  $H^\pm \rightarrow \tau^\pm \nu_\tau$  in the  $\tau + \text{jets}$  and  $\tau + \text{lepton}$  final states with  $36 \text{ fb}^{-1}$  of  $pp$  collision data recorded at  $\sqrt{s} = 13 \text{ TeV}$  with the ATLAS experiment," *JHEP*, vol. 09, p. 139, 2018. DOI: 10.1007/JHEP09(2018)139. arXiv: 1807.07915 [hep-ex].

## References iii

- [7] C. T. e. a. Potter, *Handbook of lhc higgs cross sections: 3. higgs properties: Report of the lhc higgs cross section working group*, en, 2013. DOI: 10.5170/CERN-2013-004. [Online]. Available: <http://cds.cern.ch/record/1559921>.
- [8] CMS Collaboration, "Search for charged higgs bosons in the  $H^\pm \rightarrow \tau^\pm \nu_\tau$  decay channel in proton-proton collisions at  $\sqrt{s} = 13$  tev," *Journal of High Energy Physics*, vol. 2019, no. 7, Jul. 2019. DOI: 10.1007/jhep07(2019)142. [Online]. Available: <https://doi.org/10.1007%2Fjhep07%282019%29142>.
- [9] C. Wanotayaroj, "Search for a Scalar Partner of the Top Quark in the Jets+MET Final State with the ATLAS detector," Presented 25 Oct 2016, Nov. 2016. [Online]. Available: <http://cds.cern.ch/record/2242196>.

## References iv

- [10] CERN, *Facts and figures about the lhc*, [Online]. Available: <https://home.cern/resources/faqs/facts-and-figures-about-lhc>.
- [11] E. Lopienska, “The CERN accelerator complex, layout in 2022. Complexe des accélérateurs du CERN en janvier 2022,” , Feb. 2022, General Photo. [Online]. Available: <https://cds.cern.ch/record/2800984>.
- [12] ATLAS Collaboration, *Atlas schematics*, [Online]. Available: <https://atlas.cern/Resources/Schematics>.
- [13] *Pseudorapidity*. Wikipedia, Feb. 2009. [Online]. Available: <https://en.wikipedia.org/wiki/File:Pseudorapidity2.png>.

## References v

- [14] ——, “ATLAS data quality operations and performance for 2015–2018 data-taking,” *Journal of Instrumentation*, vol. 15, no. 04, P04003–P04003, Apr. 2020. DOI: 10.1088/1748-0221/15/04/p04003. [Online]. Available: <https://doi.org/10.1088/1748-0221/15/04/p04003>.
- [15] ——, *ATLAS tile calorimeter: Technical Design Report*, ser. Technical design report. ATLAS. Geneva: CERN, 1996. DOI: 10.17181/CERN.JRBJ.7028. [Online]. Available: <https://cds.cern.ch/record/331062>.
- [16] ——, *Atlas daq approved plots*, [Online]. Available: <https://twiki.cern.ch/twiki/bin/view/AtlasPublic/ApprovedPlotsDAQ>.

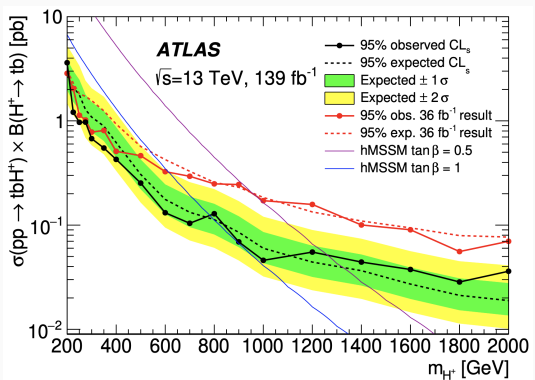
- [17] ——, “Optimisation and performance studies of the ATLAS  $b$ -tagging algorithms for the 2017-18 LHC run,”, Jul. 2017, All figures including auxiliary figures are available at  
<https://atlas.web.cern.ch/Atlas/GROUPS/PHYSICS/PUBNOTES/ATL-PHYS-PUB-2017-013>. [Online]. Available: <http://cds.cern.ch/record/2273281>.
- [18] P. O. Hansson Adrian, “The ATLAS  $b$ -jet Trigger,”, Nov. 2011, Comments: 4 pages, 6 figures, conference proceedings for PIC2011. arXiv: 1111.4190. [Online]. Available: <https://cds.cern.ch/record/1397942>.
- [19] Y. Sakurai, “The ATLAS Tau Trigger Performance during LHC Run 1 and Prospects for Run 2,” Tech. Rep., 2014, Comments: LHCP Conference 2014. arXiv: 1409.2699. [Online]. Available:  
<https://cds.cern.ch/record/1754701>.

- [20] *Classifier comparison*, [Online]. Available:  
[https://scikit-learn.org/stable/auto\\_examples/classification/plot\\_classifier\\_comparison.html](https://scikit-learn.org/stable/auto_examples/classification/plot_classifier_comparison.html).
- [21] A. Ye, *When and why tree-based models (often) outperform neural networks*, Sep. 2020. [Online]. Available:  
<https://towardsdatascience.com/when-and-why-tree-based-models-often-outperform-neural-networks-ceba9ecd0fd8>.
- [22] ATLAS Collaboration, *Public atlas luminosity results for run-2 of the lhc*, [Online]. Available:  
[https://twiki.cern.ch/twiki/bin/view/AtlasPublic/LuminosityPublicResultsRun2#Integrated\\_and\\_Instantaneous\\_Lum](https://twiki.cern.ch/twiki/bin/view/AtlasPublic/LuminosityPublicResultsRun2#Integrated_and_Instantaneous_Lum).

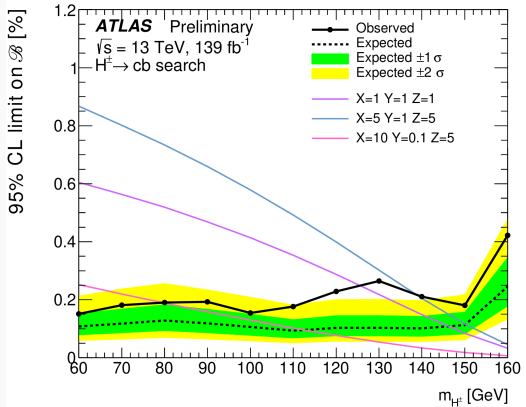
- [23] P. Baldi, K. Cranmer, T. Faucett, P. Sadowski, and D. Whiteson, “Parameterized neural networks for high-energy physics,” *The European Physical Journal C*, vol. 76, no. 5, p. 235, 2016. DOI: 10.1140/epjc/s10052-016-4099-4. [Online]. Available: <https://doi.org/10.1140/epjc/s10052-016-4099-4>.
- [24] ATLAS collaboration, “Search for charged higgs bosons decaying into a top quark and a bottom quark at  $\sqrt{s} = 13$  tev with the atlas detector,” *Journal of High Energy Physics*, vol. 2021, no. 6, p. 145, 2021. DOI: 10.1007/JHEP06(2021)145. [Online]. Available: [https://doi.org/10.1007/JHEP06\(2021\)145](https://doi.org/10.1007/JHEP06(2021)145).

- [25] “Search for a light charged Higgs boson in  $t \rightarrow H^\pm b$  decays, with  $H^\pm \rightarrow$ , in the lepton+jets final state in proton-proton collisions at  $\sqrt{s} = 13$  TeV with the ATLAS detector,” CERN, Geneva, Tech. Rep., 2021, All figures including auxiliary figures are available at  
<https://atlas.web.cern.ch/Atlas/GROUPS/PHYSICS/CONFNOTES/ATLAS-CONF-2021-037>. [Online]. Available: <https://cds.cern.ch/record/2779169>.

## Other $H^\pm$ Searches

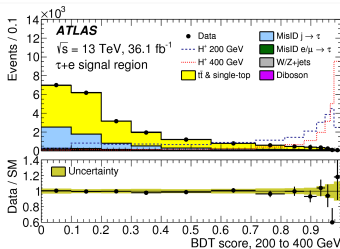
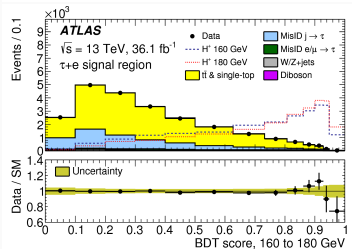
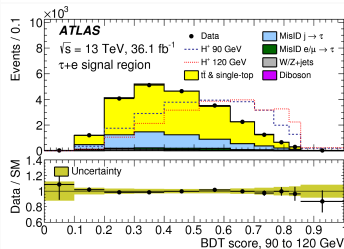
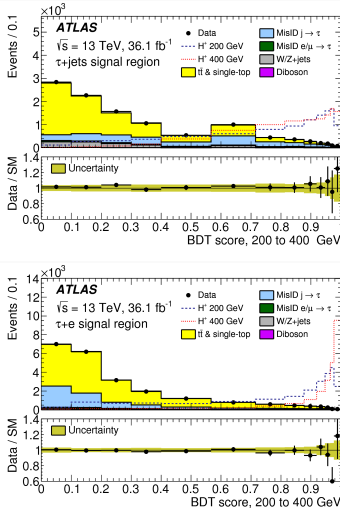
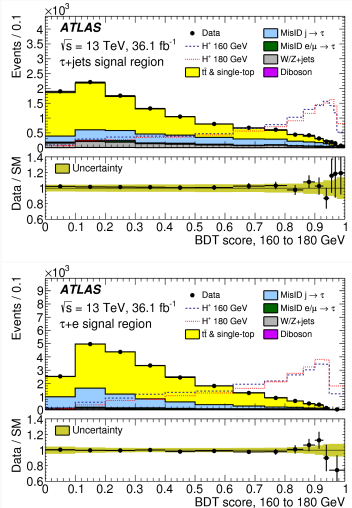
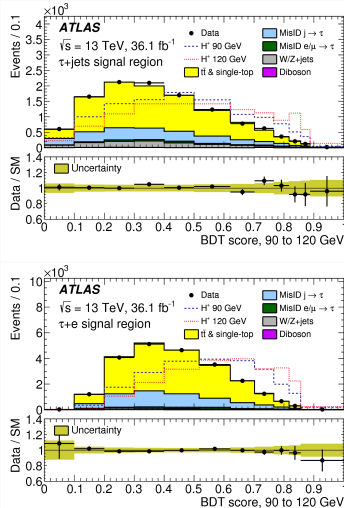


[24]

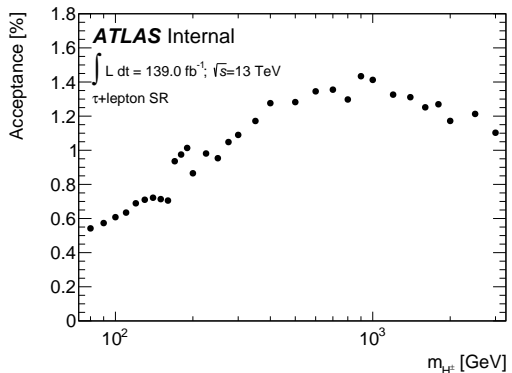
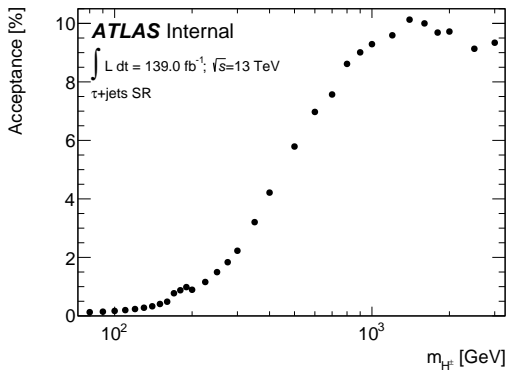


[25]

# JHEP 09(2018)139 BDT Scores in Signal Regions



# Signal Acceptance

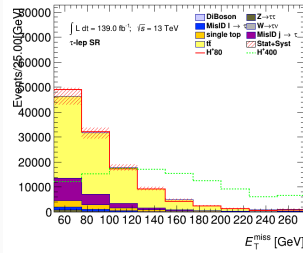
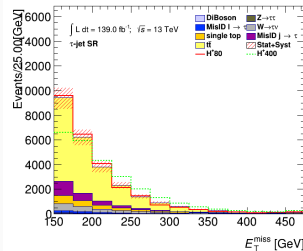


# Background Estimation

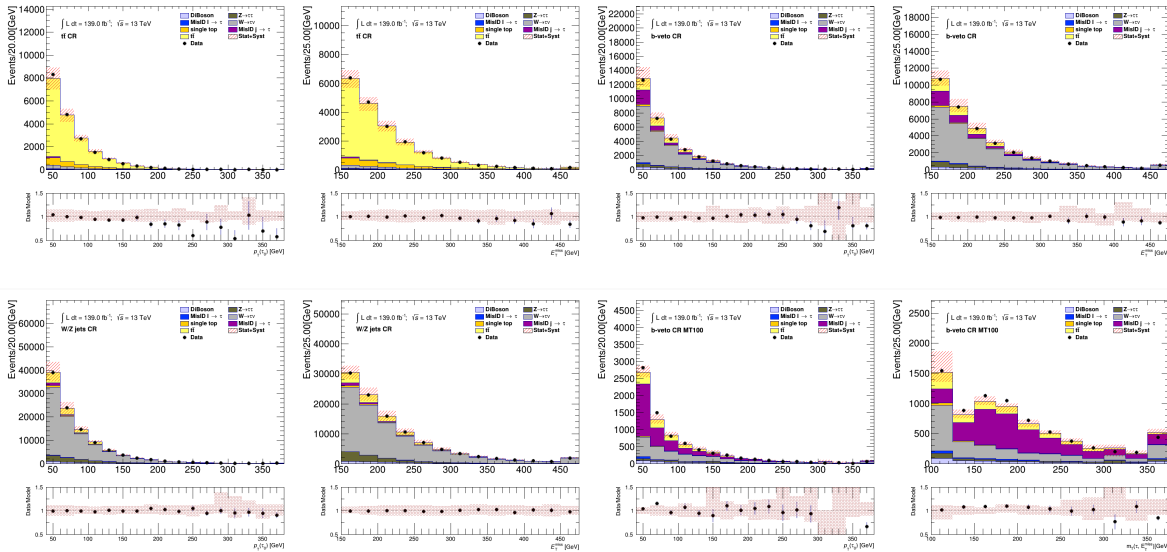
- Control regions defined to verify main sources of background

	$t\bar{t}$ CR	W+Jets CR	b-veto CR	b-veto $m_T > 100$ CR
Number of $\tau_{had-vis}$	1	1	0	0
$p_T^\tau$	> 40 GeV	> 40 GeV	> 40 GeV	> 40 GeV
Number of jets	$\geq 3$	$\geq 3$	$\geq 3$	$\geq 3$
$p_T^{jet}$	$\geq 25$ GeV	$\geq 25$ GeV	$\geq 25$ GeV	$\geq 25$ GeV
Number of b-jets	$\geq 2$	0	0	0
Number of $\ell$	0	0	0	0
$E_T^{\text{miss}}$	> 150 GeV	> 150 GeV	> 150 GeV	> 150 GeV
$m_T(\tau, E_T^{\text{miss}})$	< 100 GeV	< 100 GeV	> 50 GeV	> 100 GeV
Type of modeling	$t\bar{t}$	W+Jets	Close to SR	Fake $j \rightarrow \tau$ enriched

	Dilepton-btag CR	Zee CR	b-veto CR	Same Sign CR
Number of $\tau_{had-vis}$	0	1	0	0
$p_T^\tau$	> 30 GeV	> 30 GeV	> 30 GeV	> 30 GeV
Number of jets	$\geq 1$	$\geq 1$	$\geq 1$	$\geq 1$
$p_T^{jet}$	$\geq 25$ GeV	$\geq 25$ GeV	$\geq 25$ GeV	$\geq 25$ GeV
Number of b-jets	$\geq 1$	0	0	$\geq 1$
Number of $\ell$	2 (1 e, 1 $\mu$ )	1 e	1 tight e ( $\mu$ )	1 tight e ( $\mu$ )
$E_T^{\text{miss}}$	> 50 GeV	> 50 GeV	> 50 GeV	> 50 GeV
mass( $\tau, e$ )	N/A	> 40; < 140 GeV	N/A	N/A
Type of modeling	$t\bar{t}$ and single-top	Fake $\ell \rightarrow \tau$ enriched	Close to SR	Fake $j \rightarrow \tau$ enriched



# $\tau + \text{jets}$ Background Modeling



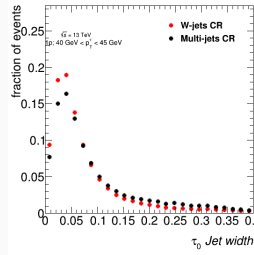
# Background Estimation: $j \rightarrow \tau$ Fakes

- Extract Fake-Factors  $FF = \frac{N_{\tau_{had-vis}}^{CR}}{N_{\bar{\tau}_{had-vis}}^{CR}}$  from two orthogonal control regions:

Multi-Jet (gluon enriched)	W+Jets (quark enriched)
$E_T^{\text{miss}}$ or Multi-Jet trigger	Single lepton triggers
$\geq 1\tau_{had}, p_T^{\tau} > 30 \text{ GeV}$	$\geq 1\tau_{had}, p_T^{\tau} > 30 \text{ GeV}$
$\geq 3$ jets	$\geq 1$ jet
0 b-jets	0 b-jets

- Combine the two Fake-Factors via the template fit method:
  - Find two separate templates for anti- $\tau$  in each CR
  - Fit both templates to the shape of the anti- $\tau$  in the SR
  - Lowest  $\chi^2$  of the fit defines  $\alpha_{MJ}$  value and the corresponding error
- Number of events with fake  $\tau$  in the signal region is given by:

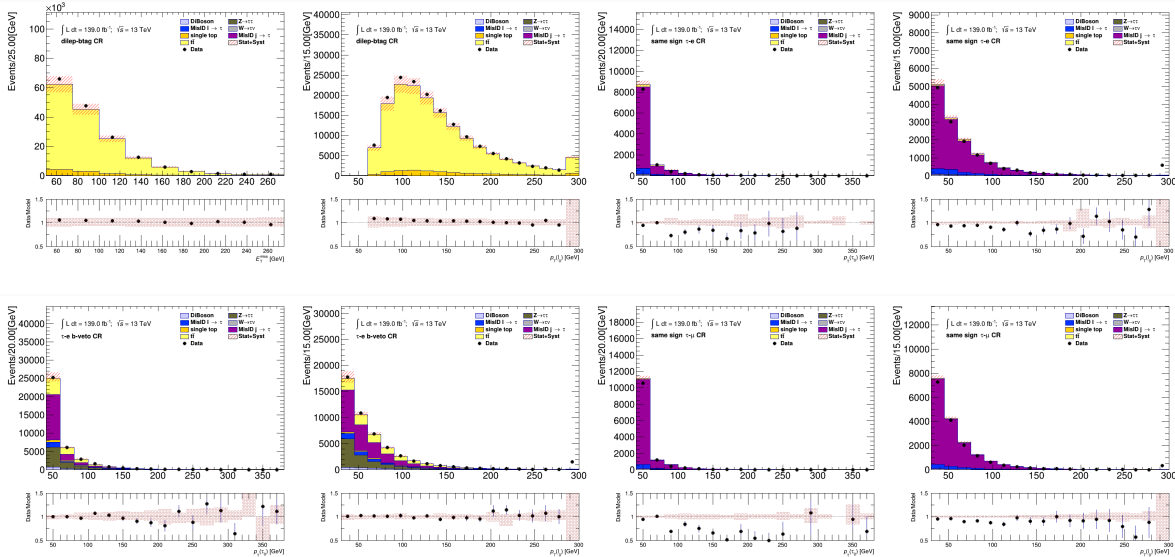
$$N_{fakes}^{Thad-vis} = \sum_i N_{\bar{\tau}_{had-vis}}^{SRi} FF_i$$



- $\bar{\tau}_0$  jet width used in  $\alpha$  fitting of 1-prong and 3-prong  $\bar{\tau}$

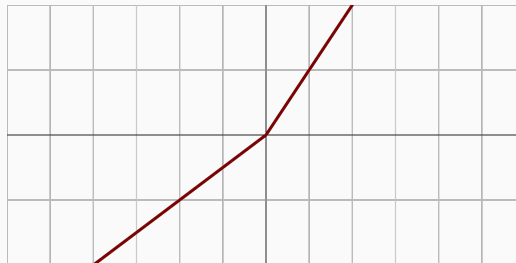
$\bar{\tau} ID$   
RNN Score > 0.01  
Not loose

# $\tau + \ell$ Background Modeling



## PNN Hyperparameter Optimization Search

- LeakyReLU activation function has an  $\alpha$  parameter
- Slope of negative portion
  - Prevents neurons from “dying” by allowing negative weight values
- Standard relu is where  $\alpha = 0$



# PNN Hyperparameter Optimization

Parameter	softsign	relu	LeakyReLU
activation function	softsign	relu	LeakyReLU
loss function	binary crossentropy	mean squared error	mean absolute error
width	32		
depth	10		

Parameter	width	8	16	32
width	8	16	32	
depth	3	5	10	
dropout	0.1	0.3		
activation function	softsign			
loss function	binary crossentropy			

Parameter	width	32	64	128
width	32	64	128	
depth	2	3	4	
dropout	0.1			
activation function	softsign	relu	LeakyReLU	
batch size	1025			
loss function	binary crossentropy			

Parameter	width	32	64	128	
width	32	64	128		
depth	2	3	4		
$\alpha$	0.01	0.05	0.001	0.005	
batch size	1024				
dropout	0.1				
activation function	LeakyReLU				
loss function	binary crossentropy				

Parameter	width	32	64	128	256
width	32	64	128	256	
depth	2	3	4	5	
batch size	1024				
dropout	0.1				
activation function	LeakyReLU				
$\alpha$	0.05				
loss function	binary crossentropy				

# PNN Hyperparameter Optimization Results

width	depth	80	150	250	500	Avg	LowMassAvg
128	3	$0.6661 \pm 0.0000$	$0.8145 \pm 0.0000$	$0.9031 \pm 0.0000$	$0.9633 \pm 0.0000$	$0.8876 \pm 0.0000$	$0.8261 \pm 0.0968$
128	5	$0.6492 \pm 0.0000$	$0.8043 \pm 0.0000$	$0.9078 \pm 0.0000$	$0.9628 \pm 0.0000$	$0.8861 \pm 0.0000$	$0.8235 \pm 0.1000$
128	4	$0.6593 \pm 0.0000$	$0.8117 \pm 0.0000$	$0.9012 \pm 0.0000$	$0.9638 \pm 0.0000$	$0.8858 \pm 0.0000$	$0.8232 \pm 0.0994$
128	2	$0.6444 \pm 0.0000$	$0.8070 \pm 0.0000$	$0.9075 \pm 0.0000$	$0.9631 \pm 0.0000$	$0.8857 \pm 0.0000$	$0.8231 \pm 0.1006$
64	4	$0.6576 \pm 0.0050$	$0.8080 \pm 0.0013$	$0.9052 \pm 0.0045$	$0.9656 \pm 0.0016$	$0.8857 \pm 0.0002$	$0.8230 \pm 0.0994$
64	2	$0.6528 \pm 0.0066$	$0.8052 \pm 0.0023$	$0.9057 \pm 0.0032$	$0.9651 \pm 0.0007$	$0.8855 \pm 0.0004$	$0.8228 \pm 0.0996$
64	5	$0.6538 \pm 0.0050$	$0.8044 \pm 0.0019$	$0.9058 \pm 0.0037$	$0.9653 \pm 0.0014$	$0.8853 \pm 0.0005$	$0.8224 \pm 0.0997$
64	3	$0.6520 \pm 0.0067$	$0.8051 \pm 0.0018$	$0.9042 \pm 0.0044$	$0.9649 \pm 0.0019$	$0.8853 \pm 0.0011$	$0.8223 \pm 0.0994$
256	5	$0.6536 \pm 0.0010$	$0.8044 \pm 0.0033$	$0.9036 \pm 0.0042$	$0.9644 \pm 0.0022$	$0.8844 \pm 0.0002$	$0.8213 \pm 0.1003$
256	4	$0.6434 \pm 0.0000$	$0.8018 \pm 0.0000$	$0.9017 \pm 0.0000$	$0.9619 \pm 0.0000$	$0.8823 \pm 0.0000$	$0.8181 \pm 0.1013$
32	3	$0.6369 \pm 0.0094$	$0.7950 \pm 0.0041$	$0.8977 \pm 0.0032$	$0.9635 \pm 0.0022$	$0.8798 \pm 0.0012$	$0.8139 \pm 0.1031$
32	4	$0.6384 \pm 0.0037$	$0.7935 \pm 0.0033$	$0.8986 \pm 0.0037$	$0.9636 \pm 0.0016$	$0.8799 \pm 0.0009$	$0.8139 \pm 0.1031$
32	2	$0.6399 \pm 0.0058$	$0.7924 \pm 0.0024$	$0.8983 \pm 0.0033$	$0.9629 \pm 0.0023$	$0.8796 \pm 0.0004$	$0.8135 \pm 0.1023$
32	5	$0.6350 \pm 0.0077$	$0.7931 \pm 0.0056$	$0.8981 \pm 0.0022$	$0.9625 \pm 0.0005$	$0.8792 \pm 0.0011$	$0.8128 \pm 0.1035$
256	2	$0.6320 \pm 0.0044$	$0.7971 \pm 0.0000$	$0.8939 \pm 0.0034$	$0.9587 \pm 0.0018$	$0.8781 \pm 0.0002$	$0.8120 \pm 0.1023$

# Fake-factor method uncertainties

Sources of systematic uncertainties associated with the FF method:

- Statistical uncertainties
- True  $\tau$  contamination in the anti- $\tau$  CR
- $\alpha_{MJ}$  fitting procedure uncertainty
- Tau RNN Identification SF variation
- Heavy flavor jet fraction

Source of uncertainty	$\tau + \text{jets}$		$\tau + \ell$	
	Effect on yield	Shape	Effect on yield	Shape
Fake factors: statistical uncertainties	3.9%	✗	3.2%	✗
Fake factors: True $\tau_{\text{had-vis}}$ in the anti- $\tau_{\text{had-vis}}$ CR	+3.4% -3.2%	✗	+4% -4.3%	✗
Fake factors: tau RNN Identification SF	2.7%	✓	2.7%	✓
Fake factors: $\alpha_{MJ}$ uncertainty	3.6%	✗	1.9%	✗
Fake factors: heavy flavor jet fraction	6%	✓	5.53%	✓

# Sources of Systematic Uncertainty

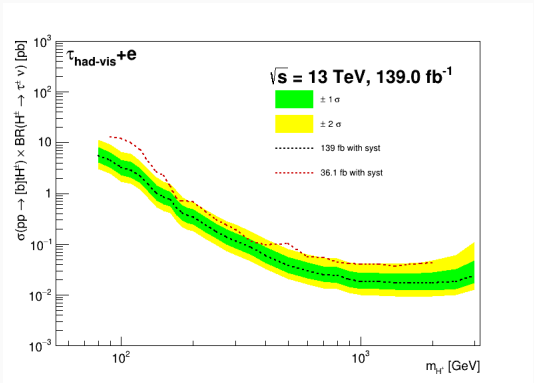
Source	Impact on the expected event yield (%)					
	$\tau$ -jets		$\tau+e$		$\tau+\mu$	
	$t\bar{t}$	$H^\pm 200 \text{ GeV}$	$t\bar{t}$	$H^\pm 200 \text{ GeV}$	$t\bar{t}$	$H^\pm 200 \text{ GeV}$
$T_{had-vis}$ reconstruction efficiency	$\pm 1.24$	$\pm 1.22$	$\pm 1.23$	$+1.22$ $-1.23$	$\pm 1.23$	$\pm 1.22$
$T_{had-vis}$ -id	$\pm 1.79$	$\pm 0.52$	$\pm 1.40$	$\pm 0.50$	$\pm 1.40$	$\pm 0.48$
$T_{had-vis}$ energy scale	$+2.53$ $-2.80$	$+2.00$ $-1.66$	$+1.60$ $-1.44$	$+1.28$ $-1.66$	$+1.53$ $-1.39$	$+1.72$ $-1.46$
$T_{had-vis}$ energy scale (detector)	$+1.96$ $-1.55$	$+1.64$ $-1.49$	$+0.23$ $-0.21$	$+1.15$ $-1.08$	$+0.16$ $-0.55$	$+0.49$ $-1.5$
$T_{had-vis}$ energy scale (in-situ)	$+144$ $-1.43$	$+0.22$ $-0.74$	$+1.17$ $-1.20$	$+0.74$ $-0.63$	$+1.14$ $-1.15$	$+0.54$ $-0.37$
$T_{had-vis}$ energy scale (model)	$+0.56$ $-0.61$	$-0.06$ $-0.21$	$+0.23$ $-0.18$	$+1.15$ $-1.08$	$+0.16$ $-0.55$	$+0.49$ $-1.50$
$T_{had-vis}$ energy scale (physics list)	$+1.27$ $-1.26$	$-0.72$ $-0.65$	$+0.74$ $-0.65$	$+0.67$ $-0.25$	$+0.72$ $-0.63$	$+0.83$ $-0.60$
jet uncertainties	$+7.38$ $-8.39$	$+6.51$ $-9.06$	$+3.41$ $-3.31$	$+4.49$ $-2.78$	$+3.18$ $-3.24$	$+3.67$ $-2.96$
$E_T^{\text{miss}}$ soft term scale/resolution	$+1.31$ $-1.12$	$+1.15$ $-1.49$	$+0.29$ $-0.24$	$+0.88$ $-0.34$	$+0.30$ $-0.23$	$+0.21$ $-0.11$
trigger	$+1.23$ $-1.61$	$\pm 0.03$	0	0	$+0.55$ $-0.56$	$\pm 56$
e-id	0	0	$\pm 0.71$	$\pm 0.73$	0	0
$\mu$ -id/reconstruction/isolation	0	0	0 $-0.01$	0 $-0.11$	$+0.97$ $-1.40$	$+1.00$ $-2.94$
$\mu$ MS	0	0	0	0	$+0.09$ $-0.12$	$+0.40$ $-0.34$

# Expected Yields

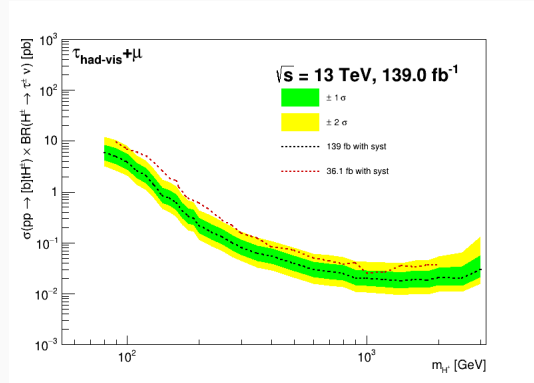
- Analysis is still blinded
  - Ongoing work with the internal ATLAS review process
- Expected number of events from each background source and two arbitrary  $m_{H^\pm}$  points
- PNN is used to separate signal from background

Sample	Event yields +jets		Event yields +e		Event yields + $\mu$				
$t\bar{t}$	18443.27	$\pm$ 48.35	+1545.67 -1697.11	43813.50	$\pm$ 76.85	+1749.82 -1833.87	44486.48	$\pm$ 75.33	+1811.78 -1907.08
Single-top-quark	2284.34	$\pm$ 17.39	+184.69 -207.49	3260.52	$\pm$ 20.81	+124.27 -134.66	3873.35	$\pm$ 22.06	+158.03 -165.92
$W \rightarrow \tau\nu$	1979.17	$\pm$ 23.63	+179.85 -229.80	2.41	$\pm$ 0.56	+0.22 -2.15	0.07	$\pm$ 0.12	+0.08 -0.16
$Z \rightarrow \tau\tau$	242.12	$\pm$ 5.50	+24.27 -32.88	913.55	$\pm$ 20.42	+64.56 -149.42	845.89	$\pm$ 22.07	+88.71 -111.03
Diboson ( $WW, WZ, ZZ$ )	133.76	$\pm$ 4.69	+9.47 -12.61	72.64	$\pm$ 1.52	+5.25 -3.91	80.81	$\pm$ 1.53	+5.40 -6.45
Misidentified $e, \mu \rightarrow \tau_{had-viz}$	328.89	$\pm$ 6.85	+25.60 -34.58	1083.97	$\pm$ 24.33	+41.65 -73.42	1060.30	$\pm$ 15.84	+43.44 -70.69
Misidentified jet $\rightarrow \tau_{had-viz}$	2506.28	$\pm$ 17.39	+130.53 -133.40	8662.43	$\pm$ 37.49	+450.65 -470.53	8426.64	$\pm$ 37.12	+440.04 -459.88
All backgrounds	25917.83	$\pm$ 59.82	+1572.87 -1730.97	57809.03	$\pm$ 93.57	+1812.82 -1846.46	58773.63	$\pm$ 90.99	+1873.75 -1970.06
$H^\pm$ (170 GeV), hMSSM $\tan\beta = 40$	1075.81	$\pm$ 9.12	+82.89 -79.19	598.17	$\pm$ 6.60	+20.84 -22.52	702.21	$\pm$ 6.93	+22.39 -16.12
$H^\pm$ (1000 GeV), hMSSM $\tan\beta = 40$	12910.36	$\pm$ 59.30	+784.57 -720.17	938.90	$\pm$ 13.25	+48.99 -37.72	1024.06	$\pm$ 13.21	+48.42 -57.01

# $H^\pm \rightarrow \tau\nu$ Expected Limits

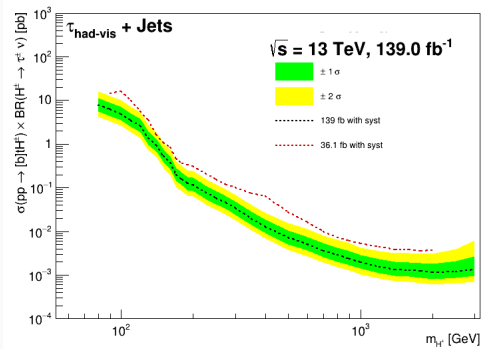


$\tau + e$

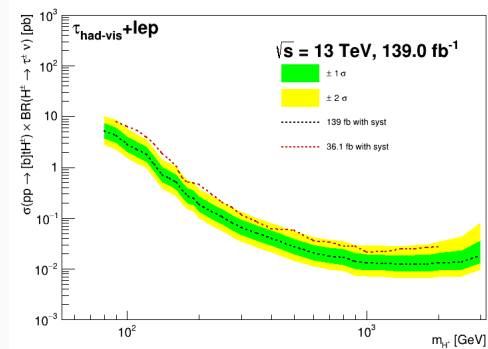


$\tau + \mu$

# $H^\pm \rightarrow \tau\nu$ Expected Limits



$\tau + jets$



$\tau + \ell$